Composite Structures 194 (2018) 345–356

Contents lists available at ScienceDirect

Composite Structures

journal homepage: www.elsevier.com/locate/compstruct

A metamodel-based optimization approach to reduce the weight of composite laminated wind turbine blades

Alejandro Albanesi[a,b,*], Nadia Roman[a,d], Facundo Bre[a,c], Victor Fachinotti[a]

[a] CIMEC Centro de Investigación de Métodos Computacionales, UNL, CONICET, Col. Ruta 168 s/n, Predio Conicet Dr Alberto Cassano, 3000 Santa Fe, Argentina
[b] Grupo de Investigación en Mecánica Aplicada (GIMA), FRSF, UTN, 3000, Lavaise 610, Santa Fe, Argentina
[c] Grupo de Investigación en Mecánica Computacional y Estructuras (GIMCE), FRCU, UTN, 3260, Ing. Pereyra 676, Concepción del Uruguay, Argentina
[d] Grupo de Investigación en Métodos Numéricos en Ingeniería (GIMNI), FRSF, UTN, 3000, Lavaise 610, Santa Fe, Argentina

ARTICLE INFO

Keywords:
Optimization
Artificial neural network
Genetic algorithm
Composite materials
Wind turbine blade

ABSTRACT

In wind turbine blades, the complex resultant geometry due to the aerodynamic design cannot be modified in the successive mechanical design stage. Hence, the reduction of the weight and manufacturing costs of the blades while assuring appropriate levels of structural stiffness, integrity and reliability, require a composite material layout that must be optimally defined.

The aim of this work is to present a metamodel-based method to optimize the composite laminate of wind turbine blades. This methodology combines a genetic algorithm (GA) with an artificial neural network (ANN) in order to reduce the computational cost of the optimization procedure. Therefore, at first, representative samples were built to train and validate the ANN model, and then, the ANN model is coupled with GA to find the optimal structural blade design. As an actual case study, the method was applied to redesign a medium-power 40-kW wind turbine blade to reduce its mass while structural and manufacturing constrained are fulfilled.

The results indicated that is possible to save of up to 20% of laminated mass compared to a reference design. Furthermore, a 40% reduction of the computational cost was achieved in contrast with the typical simulation-based optimization approach.

1. Introduction

In the design process of laminated wind turbine blades, where the geometry of the blades cannot be modified due to aerodynamic reasons, the reductions of rotor weight and costs while maintaining adequate levels of structural stiffness and reliability, leads to a composite material layout that must be optimally defined. This design problem can be stated as finding the proper variable stiffness laminate that minimizes the weight of the blades while satisfying a series of design constraints that include mechanical and manufacturing issues [1]. Given the large number of design variables involved, the classical approach consists in simulation-based optimization, which requires the use of an optimization algorithm to handle variables and constraints, and a mechanical model to compute the structural response of the blade. Genetic algorithms (GA) are based in the nature principal of "survival of the fittest", and they are intensively used in the optimization of the stacking sequence of laminated composites due to their global searching capability and discrete variable handling [2,3]. However, the main disadvantage of simulation-based optimization approach is the computational cost of each simulation analysis, so it becomes a large time-consuming process.

Artificial Neural Networks (ANNs) are models capable of mapping non-linear relationships between a large number of inputs and outputs, solving non-linear problems with very low computational time. With the correct number of sampling points, ANNs are able to reproduce the structural response of composite structures in less time compared to numerical simulations [4], and for this reason, have become frequently used in the design and optimization of composite structures.

Among design procedures of composites using ANN, Yan et al. [5] used ANN to predict bond strength in glass fiber reinforced concrete beams in which the neural network was trained with a table of normalized bond strengths, and then GA was launched to optimize the weights and biases of the ANN using as fitness function the difference between predicted and actual values. Artero-Guerrero et al. [6] studied the influence of the stacking sequence on the ballistic limit for composite plates using an ANN model. The ANN model was trained with both experimental data obtained from high-velocity impact tests and numerical results through simulation. The results indicated an increase of 40% for the ballistic limit without increasing the weight of the

* Corresponding author at: CIMEC Centro de Investigación de Métodos Computacionales, UNL, CONICET, Col. Ruta 168 s/n, Predio Conicet Dr Alberto Cassano, 3000 Santa Fe, Argentina.
E-mail address: aalbanesi@cimec.unl.edu.ar (A. Albanesi).

https://doi.org/10.1016/j.compstruct.2018.04.015
Received 13 January 2018; Received in revised form 28 February 2018; Accepted 2 April 2018
Available online 07 April 2018

composite plates. Balokas et al. [7] presented a multiscale analysis to determine the elastic properties for braided composite materials under uncertainty due to manufacturing processes, by training an ANN with a probabilistic FEM method that accounts for the prediction of elastic properties under random uncertainties. These authors reported a reduction by orders of magnitude in the computational cost of the procedure.

ANNs also have a vast field of application in the optimization process of composite materials. Bisagni and Lanzi [8] developed one of the pioneering single objective optimization procedures, which combines an ANN and GA in order to design stiffened composite panels under compressive loads. The stacking sequence of the skin and stiffeners of the panel were the designed variables, and the objective function consisted in the weight of the panel subjected to post-bucking constraints. The authors reported a weight reduction of 18% and time-saving of over 90% in the optimization process (without considering training and evaluation). Another single objective optimization procedure combining ANN with GA was presented by Fu et al. [9] to design woven composite stiffened panels. A prior multi-scale analysis had been performed to predict the macroscale behavior of the woven composite and to determine the elastic properties of the material. The objective function was the weight of the panels subject to buckling and post bucking constraints. Mass savings of 26% were achieved with the proposed methodology.

As for multi-objective optimization of composite materials, Abouhamze and Shakeri [10] performed the multi-objective optimization of cylindrical panels using ANN and GA. The optimal angle of the stacking sequence was determined in an optimization strategy considering the first natural frequency and the critical buckling load as equally important objective functions. This work reported that the computational cost of the optimization process was reduced from 155 min to 55 s. Marín et al. [11] carried out the multi-objective optimization of composite panels under mechanical and hygrothermal loads using ANN and GA. The weight, stresses, and strains due to hygrothermal expansion in the panels were equally important objective functions. The authors reported a reduction of more than 90% in the computational cost of the optimization process.

In a previous work [12], we described the simulation-based optimization process for the blades of a 40-kW three-blade horizontal axis wind turbine (HAWT), combining GA and the Inverse Finite Element Method (IFEM) for structural analysis. The optimal number and order of plies in tapered laminates were the design variables, and the objective function consisted in the minimum mass of the blade subjected to displacement, stress, vibration and manufacturing constraints. A crucial contribution is the use of IFEM [13,14] for the structural analysis, allowing the designer to account for the shape the laminates are expected to attain after large elastic deformations: the blades have to attain a given aerodynamically efficient shape when they are deformed by the service loads.

The aim of this current work is to present a metamodel-based method that combines an ANN model with GA to optimize the composite laminate of wind turbine blades, in order to reduce significantly the computational cost of the optimization procedure. Firstly, representative samples were built to train and validate the ANN model in order to replace the IFEM simulations, and then, the ANN model was coupled with GA to find the optimal structural blade design. The objective function was the minimization of the mass of the blades, subject to four constraints: allowable tip deflection, the maximum stress criteria, natural vibration frequencies, and a maximum number of successive identical plies. As in our former work [12], design variables consisted in the number and order of plies in the tapered composite laminates.

This paper is organized as follows: Section 2 presents the case study, and describes the geometry and material layout of the reference blade, the external loads acting over the blades, and the mechanical properties of the composite materials adopted. Section 3 is the main core of this work, and presents the optimization problem, the full procedure used to combine ANN with GA, the description of the IFEM structural solver, and the training and validation of the ANN. Numerical results are given in Section 4, and the concluding remarks in Section 5.

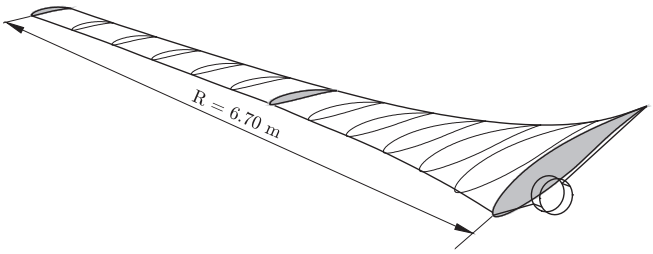

Fig. 1. Geometry of the reference blade, determined in [12].

2. Case study

Let us consider as a case study a 6.70 m long wind turbine blade that belongs to a 40 kW three-blade HAWT, designed in our previous work [14] and depicted in Fig. 1. The turbine rotates at 72 RPM with a wind velocity of 7 m/s. The geometry of the blade is defined by three main airfoils from the SG604X family [15]: (SG6040) at the root, (SG6042) at mid-span and (SG6043) at the tip, and a linear interpolation is used between these sections. The adimensional chord length and the twist angle distribution are presented in Table 1 for the adimensional blade span.

2.1. Laminate composite material of the reference blade

The composite laminate material of the reference blade consists of multiple plies of E-type glass fibers and epoxy resin, with a volume fraction of 60%. The blade is divided into 10 regions and a maximum of 11 laminate plies are allowed in the shell skin, as shown in Fig. 2. Double-bias, biaxial and uniaxial fiberglass are considered, and the final outer ply is always made of epoxy gelcoat. The lamination sequence is uniform in each region [3], and ply drops are also allowed between regions. The stacking sequence is repeated at the lower and upper side (i.e., it is symmetric with respect to the core of the blade). The material properties are listed in Table 2.

2.2. External loads over the blades

The service loads acting over the blades are a combination of the *resultant aerodynamic forces* and the *stationary inertial loads*. The resultant aerodynamic forces due to the pressure gradients and viscous flow have been computed in [14] with Computational Fluid Dynamics

Table 1
Chord length and twist angle distribution along the adimensional blade span.

Blade span [r/R]	Chord [c/R]	Twist [degrees]
0.12	0.170	28.51
0.19	0.140	19.08
0.27	0.118	13.49
0.35	0.090	9.95
0.42	0.080	7.59
0.50	0.070	5.93
0.58	0.060	4.72
0.65	0.055	4.12
0.73	0.050	3.72
0.81	0.045	3.43
0.88	0.041	3.31
0.96	0.039	3.25
1.00	0.038	3.25

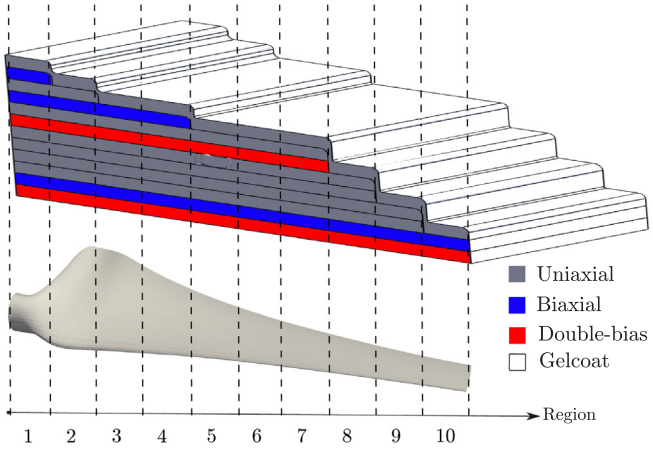

Fig. 2. Composite layout of the reference blade [12]. The blade is divided into 10 regions and a maximum of 11 laminate plies are allowed in the shell skin. The outer ply is always made of epoxy gelcoat.

Table 2
Mechanical properties of the composite materials, made of E-type glass fibers and epoxy resin, with a volume fraction of 60%.

Property	Uniaxial	Biaxial	Double bias	Gelcoat
Longitudinal elastic modulus E_X [GPa]	44	44	44	5
Transverse elastic modulus E_Y [GPa]	12.6	44	44	5
Shear modulus G_{XY} [GPa]	10	35	15	1.8
Density [Kg/m^3]	1117	1004	914	650
Poisson ratio	0.32	0.36	0.36	0.4
Thickness [mm]	0.50	0.50	0.35	0.25
Long. tensile strength X_T [MPa]	1020	1020	850	–
Long. compressive strength X_C [MPa]	610	610	550	–
Transverse tensile strength Y_T [MPa]	41	1020	850	–
Transverse compressive strength Y_C [MPa]	140	610	550	–
Shear strength S [MPa]	72	95	76	–

(CFD) using the finite volume method as implemented into the open-source software OpenFoam. The steady-state solver for incompressible and turbulent flow *simpleFoam* with the k-ω turbulence model was used along with the multiple reference frame approach trough the *fvOptions*. The boundary conditions are prescribed wind velocity at the inlet, a uniform atmospheric pressure in the lateral surface (open boundary) and in the outlet boundary, and the surface of the blades is assumed to be a smooth no-slip wall. As for the body forces, the material distribution throughout the blade in combination with the angular velocity determines the stationary inertial loads.

3. Methodology

In this section, the proposed methodology is presented. Firstly the optimization problem is detailed, including the design variables and both the manufacturing and mechanical constraints. Secondly, the simulation-based and metamodeling optimization approaches for solving the problem are explained. Thirdly, the proposed methodology is expounded, detailing the general procedure, the IFEM structural solver used for the simulations, and the training and validation of the metamodel.

3.1. Optimization problem

The optimization consists in the reduction of the mass of the blade. Given a function w describing the mass, the following optimization problem is stated:

$$\min_{\boldsymbol{x}\in\mathscr{X}} w(\boldsymbol{x}), \tag{1}$$

where $\boldsymbol{x}$ is the set of variables defining the ply layout of the composite material, and $\mathscr{X}$ is the known analysis domain which is described in Section 3.5.

3.1.1. Design variables

Given the description of the laminate in Section 2.1 and following the same convention used in [14,12], all the plies are assumed to start at the root of the blade, and the outer ply is always made of gelcoat.

Since a maximum of 11 plies are considered, the optimization of the blade is based on 22 integer variables. The set m_i, with i = 1,2,...11, denote the material in ply i, in which $m_i = 0$ is an empty ply, $m_i = 1$ is a ply made of uniaxial fiberglass, $m_i = 2$ is biaxial fiberglass, and $m_i = 3$ is double-bias fiberglass. The set d_i, with i = 1,2,...11, denote the end region of the ply i, with $1 \leqslant d_i \leq 10$ given that the blade is divided in 10 regions.

Two important aspects of this parameterization are that fiber continuity is ensured since any ply with $m_i > 1$ starts at the root and is dropped at the end of the region r_i. Also, the ply order, ply number, and ply drops are simultaneously optimized.

3.1.2. Design constraints

The constraints of the optimization problem consider geometrical aspects of the laminate (manufacturing constraints) and the mechanical performance of the blade (mechanical constraints).

Given the vector of design variables x_i, the material type m_i, the region r_i, and maximum number of plies of the same material $s_{\max}$, the *manufacturing constraints* can be stated as follows:

- At least three plies along the entire span length of the blade must exists:

$$1 \leqslant x_i \equiv m_i \leqslant 3, \quad x_{11+i} \equiv r_i = 10, \quad \text{for } i = 1,2,3. \tag{2}$$

- At most three identical plies can be placed sequentially in any angle direction:

$$c_1(\boldsymbol{x}) = s_{\max}(\boldsymbol{x}) - 3 \leq 0. \tag{3}$$

The constraint in Eq. (2) is implemented to save computational time and to reduce the amount of impractical solutions. To decrease the transverse shear stress between plies, a maximum of three identical plies can be placed sequentially in any angle direction. Hence, the nonlinear and non-differentiable integer inequality constraint of Eq. (3) is prescribed [16–18]. With these manufacturing constraints under consideration, the integer design variables are presented in Table 3.

As for the *mechanical constraints* that measure the performance of the blade, three parameters are considered:

- The maximum tip displacement of the blade should not exceed the tip displacement for the reference blade designed in [14], which is $u_{\max} = 0.350$ m. Thus the following nonlinear inequality constraint is defined:

$$c_2(\boldsymbol{x}) = u_{\text{tip}}(\boldsymbol{x}) - u_{\max} \leqslant 0, \tag{4}$$

- Being the rotational frequency of the rotor $f_{\text{rotor}} = 72$ RPM $= 1.2$ Hz, the natural frequency of the blade should be separated $\pm 5\%$ from f_{rot} as well as from $3f_{\text{rot}}$ (since there are 3 blades in the turbine), to avoid that the blades interact with each other in a similar range of frequencies of the structure as a whole. These following nonlinear inequality constraints are defined by:

Table 3
Description and bounds of the discrete design variables, considering the manufacturing constraints. Ply 1 always denotes the inner core layer, and the outer ply is made of epoxy gelcoat. For variable m_i,$m_i = 0$ is an empty ply, $m_i = 1$ is uniaxial, $m_i = 2$ is biaxial, and $m_i = 3$ is double-bias. Since the blade is divided into 10 region, variable d_i is the end region of the ply i, with $1 \leqslant d_i \leq 10$.

Description	Variable	Domain
Material in layer 1	m_1	[1–3]
Material in layer 2	m_2	[1–3]
Material in layer 3	m_3	[1–3]
Material in layer 4	m_4	[0–3]
Material in layer 5	m_5	[0–3]
Material in layer 6	m_6	[0–3]
Material in layer 7	m_7	[0–3]
Material in layer 8	m_8	[0–3]
Material in layer 9	m_9	[0–3]
Material in layer 10	m_{10}	[0–3]
Material in layer 11	m_{11}	[0–3]
Extension of layer 1	d_1	[10]
Extension of layer 2	d_2	[10]
Extension of layer 3	d_3	[10]
Extension of layer 4	d_4	[1–10]
Extension of layer 5	d_5	[1–10]
Extension of layer 6	d_6	[1–10]
Extension of layer 7	d_7	[1–10]
Extension of layer 8	d_8	[1–10]
Extension of layer 9	d_9	[1–10]
Extension of layer 10	d_{10}	[1–10]
Extension of layer 11	d_{11}	[1–10]

$$c_3(\boldsymbol{x}) = 0.05 f_{\text{rot}} - |f_{\text{blade}}(\boldsymbol{x}) - f_{\text{rot}}| \geqslant 0, \tag{5}$$

$$c_4(\boldsymbol{x}) = 0.05 f_{\text{rot}} - |f_{\text{blade}}(\boldsymbol{x}) - 3 f_{\text{rot}}| \leqslant 0, \tag{6}$$

- Each ply in the laminated composite material verifies the maximum stress failure criterion [19–21], leading to the following nonlinear and non-differentiable inequality constraints:

$$c_5^{(i)}(\boldsymbol{x}) = -k\min(\sigma_1^{(i)}(\boldsymbol{x})) - X_C^{(i)} \leqslant 0, \tag{7}$$

$$c_6^{(i)}(\boldsymbol{x}) = k\max(\sigma_1^{(i)}(\boldsymbol{x})) - X_T^{(i)} \leqslant 0, \tag{8}$$

$$c_7^{(i)}(\boldsymbol{x}) = -k\min(\sigma_2^{(i)}(\boldsymbol{x})) - Y_C^{(i)} \leqslant 0, \tag{9}$$

$$c_8^{(i)}(\boldsymbol{x}) = k\max(\sigma_2^{(i)}(\boldsymbol{x})) - Y_T^{(i)} \leqslant 0, \tag{10}$$

$$c_9^{(i)}(\boldsymbol{x}) = -k\min(\tau_{12}^{(i)}(\boldsymbol{x})) - S_\tau^{(i)} \leqslant 0, \tag{11}$$

$$c_{10}^{(i)}(\boldsymbol{x}) = k\max(\tau_{12}^{(i)}(\boldsymbol{x})) - S_\tau^{(i)} \leqslant 0, \tag{12}$$

where $X_T^{(i)}$ is the ultimate longitudinal tensile strength, $X_C^{(i)}$ is the ultimate longitudinal compressive strength, $Y_T^{(i)}$ is the ultimate transverse tensile strength, $Y_C^{(i)}$ is the ultimate transverse compressive strength, and $S_\tau^{(i)}$ is the ultimate shear strength, which are properties of the material m_i (see Table 2).

3.2. Simulation-based optimization approach

An approach commonly used to solve engineering design problems such as (1) is the simulation-based optimization. In this procedure, an optimization algorithm is directly coupled with a numerical simulation where the later has the function to evaluate the performance of the current design and the optimization algorithm, through iterative tasks, has to find a new design that improves the performance of the current one. Due to the integer nature of the design variables $\boldsymbol{x}$, non-convexity of the problem, and the non-differentiability of the objective function and most of the constraints, meta-heuristic algorithms are most suitable for the solution of the optimization problem (1). One of the most popular optimization solvers is the genetic algorithm, and it has been used by several authors to solve composed laminates problems; such as the optimal design of tapered laminates [22,23] including wind turbine blades [24]. Furthermore, some of them are implemented to tackle integer design variables [25,26].

In a previous work [12], we used the simulated-based approach to solve the same problem (1), coupling the IFEM solver with a sophisticated version of GA specially made to take into account integer and mixed integer design variables. Herein, the same version of GA based on the operators Laplace crossover and the power mutation proposed by Deep [27] is used.

3.3. Metamodeling using Artificial Neural Networks (ANNs)

Although GAs showed to be a robust tool to solve complex problems, it has a major limitation that they require hundreds or sometimes thousands of evaluations to reach optimal solutions. When the evaluation of the objective function is performed by time-costly simulations the optimization becomes a hard task. A way to improve this drawback is to parallel the evaluations of the population individuals in different computer cores [28], which is an advantage available for GAs. Whereas this method save computational time, it does not decrease the number of evaluations, and this is only achieved if a massive parallel computer is available. An alternative technique is to replace the time-costly simulations of the complex model for a metamodel (model of a model). In this case, a small set of the full model simulations is used to build a new simpler model, reducing the time of the objective function evaluation and also the total number of simulation needed.

Despite metamodels are an approximate technique, one of them, like artificial neural networks (ANNs), demonstrated to have a reliable accuracy to replace the complex model. ANNs have been recommended [29] for nonlinear very large problems with a high computational expense, such as (14). ANNs are parallel computational models inspired in the performance of the human brain that consist in an arrangement of interconnected processing units called neurons, used for tasks such as function approximation, filtering and pattern association or recognition [30]. In order to accomplish their objective, the ANNs perform a process of supervised or unsupervised learning, depending on the type of ANN and the available data (sets of inputs-outputs or sets of only inputs).

The type of ANN to implement depends on the type of problem to solve: feedforward ANNs for non linear input-output mapping of general nature or pattern association, recurrent ANNs for control, convolutional ANNs for pattern classification, adaptative ANNs for signal processing, among others [30,31]. As it was mentioned before, the purpose of the ANN models is to substitute the IFEM simulations in the optimization problem, thus they are used as a function approximation. Hence, a multilayer feedforward ANN, as shown in Fig. 3, has been adopted in this work.

Multilayer feedforward ANNs have been widely employed in the context of layered composite materials. For example, Yan et al. [5] predicted bond strength in glass fiber reinforced concrete beams, Artero-Guerrero et al. [6] analized the ballistic limit for composite plates, Balokas et al. [7] determined the elastic properties for braided composite materials, Bisagni and Lanzi [8] reproduced the global behavior of a structure in a single objective optimization procedure, Fu et al. [9] analized the structural response of a woven composite stiffened panel, Abouhamze and Shakeri [10] determined the first natural frequency

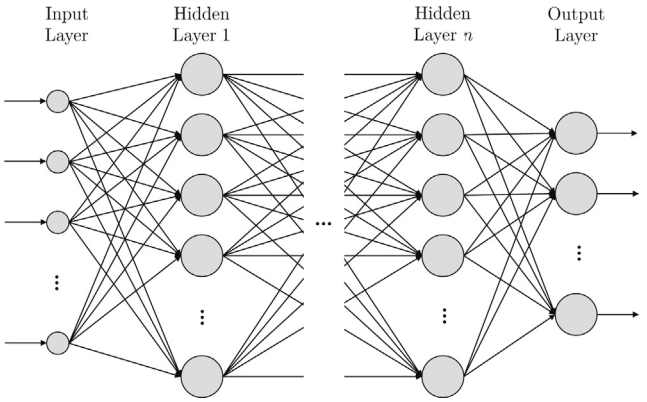

Fig. 3. Artificial Neural Network model implemented in this work.

and the critical buckling load of cylindrical panels, and Marín et al. [11] modeled the mechanical response of composite panels under mechanical and hygrothermal loads.

The architecture of this networks is formed by several layers of neurons put one after another in order that the outputs of one layer become the inputs of the following one. The first and last layers of the ANN are the Input and Output Layer, while the ones in between are called Hidden Layers.

According to the description proposed by Haykin [30], the neurons of the ANNs are characterized by the inputs signals x_i, a set of synaptic weights w_{ki}, a bias b_k, a summing junction or adder $\sum$, an activation function $\varphi(\cdot)$ and the output y_k, as it is seen in Fig. 4.

The input signals are, depending on the layer in which the neuron is located, the inputs of the problem or the output of a neuron in a previous layer. The synaptic weights measure the contribution of each input to the neuron and might take positive or negative values. The bias of the neuron increase or lower the input of the activation function. The summing junction constitutes a linear combiner of the weighted input signals: $\sum_{i=1}^{n} x_i w_{ki}$, where $i = 1,...,n$ indicates the corresponding input or synaptic weight of the k neuron. The activation function limits the amplitude of the output of the neuron described by $y_k = \varphi(u_k + b_k)$, being the basic ones the threshold function, the piecewise-linear function, and the sigmoid function.

With regard to the learning procedure of the ANN, it can be summarized in three steps [30]: the stimulation of the ANN by an environment, the changes in its free parameters (synaptic weights and bias) as a result of the stimulation, and a response in a new way to the environment due to the changes that have occurred in its internal structure. In other words, the ANN performs a training process in which it learns, by being exposed to a set of inputs and outputs, how to respond to new data. The commonly used training algorithm in multilayer feedforward networks is the backpropagation one.

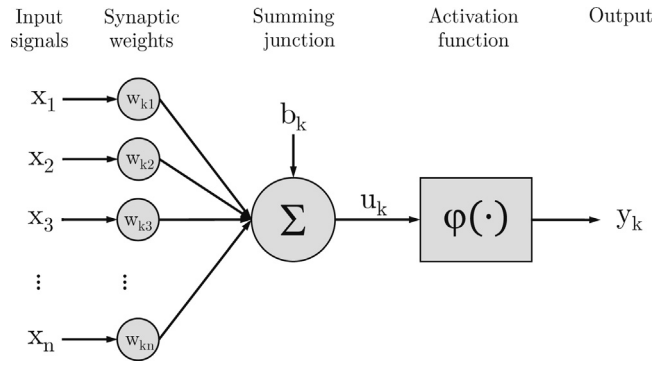

Fig. 4. Model of a neuron.

3.4. Proposed methodology

The proposed methodology for this work is depicted in Fig. 5, in which the complete process from the creation of the samples to the obtaining of the optimal solution is schematized. In order to replace the IFEM simulation implemented in [12] with a metamodel, the first step (box 1 in the figure) is to create the samples to train and validate the metamodel by the implementation of the Latin Hypercube Sampling (LHS) technique. After the inputs of the sample were obtained, they were simulated with the IFEM algorithm to obtain the outputs needed for the training and validation of the ANNs.

In the second step (box 2 in the figure), the different ANNs models were trained according to the architectures proposed in Table 4. The validation sample was used to choose the ANN model that had the best performance (lowest MSE and/or maximum correlation factor R).

In the third and last step (box 3 in the figure), the optimization was performed by the implementation of the GA algorithm described in Section 3.2. In order to validate the process, the optimal solution found was simulated with IFEM to obtain the structural response of the blade. In the case that the error between the solution obtained with GA + ANN and IFEM was small enough, the process could be finished; if not, more ANN models should have been trained.

3.5. Simulation using IFEM structural solver

The IFEM solver is able to predict the blade structural behavior given a state of loads. It computes all of the design constraints: the maximum allowable tip deflection, the maximum stress criteria, and the vibration frequency of the blades. The most outstanding feature of IFEM is that it is able to determine the unloaded manufacturing shape of the blade such that, under service loads, the deformed blade attains its efficient aerodynamic shape (that given by Fig. 1). Hence, the analysis domain consists in the shape of the blade after elastic deformations caused by the service loads. Other analysis data are the multilayer composite materials layout in the blade, and the total service loads (given by the combination of the aerodynamic and stationary inertial loads). IFEM then computes the manufacturing shape of the blade, solving a nonlinear equilibrium equation only once.

Our IFEM model is the inverse counterpart of the widely known MITC4 shell finite element [32], a quadrangle with nodes located at its vertices that uses the MITC (mixed interpolation of tensorial components) technique to avoid shear locking by replacing some components of the covariant strain fields by “assumed” strain fields. It is based in the degenerated solid approach for shells in which governing equations are the same as those for general solids, and it is capable of representing thin to moderately thick shells with multiple layers of transversely orthotropic materials due to the Mindlin-Reissner shell theory consideration. Since the IFEM solver has been thoroughly described in our previous works [14,12], only a very brief outline is presented here.

In the classic direct problem in elasticity, the undeformed configuration $\mathscr{B}^0$ depicted in Fig. 6, and the external loads responsible for deforming the shell from $\mathscr{B}^0$ to $\mathscr{B}$ through the transformation χ, are assumed to be known. Hence, the nonlinear equilibrium equation for direct FEM degenerated-solid shells can be expressed as follows:

$$\boldsymbol{R}(\boldsymbol{x},\boldsymbol{X}) = \int_{\mathscr{B}^0} \boldsymbol{B}^T(\boldsymbol{x},\boldsymbol{X})\boldsymbol{S}(\boldsymbol{E}(\boldsymbol{x},\boldsymbol{X}))dV + \boldsymbol{F}_{ext}(\boldsymbol{x},\boldsymbol{X}) = \boldsymbol{0}, \tag{13}$$

where $\boldsymbol{X}$ is the position of any point in $\mathscr{B}^0$ with midsurface $\mathscr{S}^0$,$\boldsymbol{x}$ is the position of any point in $\mathscr{B}$ with midsurface $\mathscr{S}$,$\boldsymbol{E}$ Green-Lagrange strain tensor that accounts for the deformation of the shell, $\boldsymbol{S}$ is the second Piola Kirchoff stress tensor, $\boldsymbol{F}_{ext}$ is the vector of external loads assumed to be lumped at the nodes.

In IFEM, the loaded configuration $\mathscr{B}$ as well as the external loads, responsible for deforming the shell from $\mathscr{B}^0$ to $\mathscr{B}$ through the transformation χ^{-1}, are the variables assumed to be known (see Fig. 6). Since $\mathscr{B}$ is the known domain, the vector of internal loads at each finite

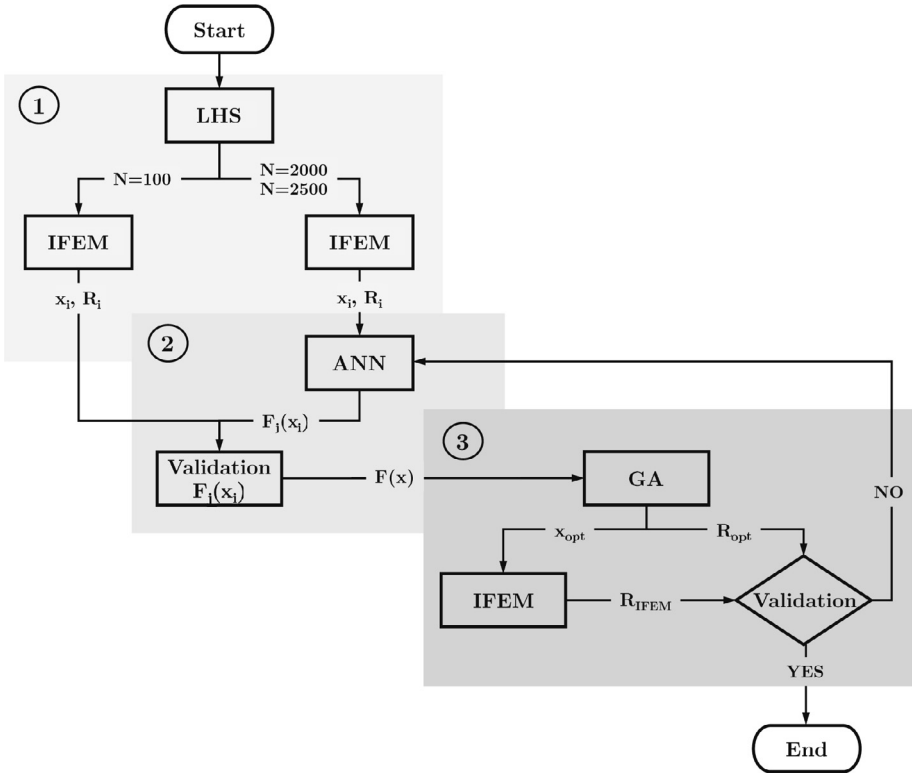

Fig. 5. Flowchart of the procedure. The first step (box 1) is the sampling and numerical simulation to feed the ANN, the second step (box 2) is the training and validation of the ANN, and the third step (box 3) is the optimization process by combination of GA + ANN.

Table 4
Architecture, configuration and parameters of the ANNs trained.

Type of ANN	Multilayer feedfoward
Training data size	2000 and 2500
Validation data size	100
Hidden layers	2
Neurons per layer	20 to 30 in Hidden Layers and 4 in Output Layer
Training function	Bayesian regularization backpropagation
Activation function	Hyperbolic tangent sigmoid for Hidden Layers, Linear for Output Layer
Performance function	Mean Squared Error (MSE)
Training stop criteria	$MSE = 1 \times 10^{-5}$
Maximum iterations	500

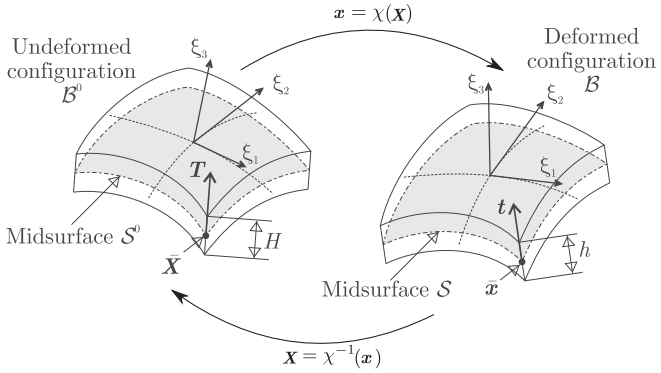

Fig. 6. Undeformed and deformed configurations of a shell.

element $\int_{\mathscr{B}^0} F\,dV = \int_{\mathscr{B}} f\,dv$, with $f = FJ^{-1}$, where J is the Jacobian determinant of the transformation from $\mathscr{B}^0$ to $\mathscr{B}$. At this point, we make use of the close relationship between FEM and IFEM: both have the identical governing equation that is given by the discrete equilibrium Eq. (13), differing only in the fact that knowns and unknowns are interchanged.

$$\boldsymbol{R}(\boldsymbol{x},\boldsymbol{X}) = \int_{\mathscr{B}} \boldsymbol{B}^T(\boldsymbol{x},\boldsymbol{X})\boldsymbol{S}(\boldsymbol{E}(\boldsymbol{x},\boldsymbol{X}))\frac{1}{J(\boldsymbol{x},\boldsymbol{X})}dV + \boldsymbol{F}_{ext}(\boldsymbol{x},\boldsymbol{X}) = \boldsymbol{0}, \tag{14}$$

This is a nonlinear equation to be solved using the Newton-Raphson method: At the iteration $i+1$,$\boldsymbol{X}$ is updated by solving the linear equation for $\Delta\boldsymbol{X}$:

$$\boldsymbol{R}(\boldsymbol{x},\boldsymbol{X}^{(i+1)}) = \boldsymbol{R}(\boldsymbol{x},\boldsymbol{X}^{(i)}) + \frac{\partial}{\partial \boldsymbol{X}}\boldsymbol{R}(\boldsymbol{x},\boldsymbol{X}^{(i)})\Delta\boldsymbol{X} = \boldsymbol{0}, \tag{15}$$

where $\frac{\partial}{\partial \boldsymbol{X}}\boldsymbol{R}(\boldsymbol{x},\boldsymbol{X}^{(i)})$ is the tangent stiffness matrix (see [13] for details).

A series of mechanical, and numerical tests assure the feasibility of the IFEM solution, and include (*i*) a topological test for detecting interpenetrated elements, (*ii*) a mechanical test to verify the validity of the hypothesis of elasticity, and (*iii*) a numerical test to verify the uniqueness of the solution (including a test for unstable equilibrium states such as buckling phenomena). If these tests are successful, the IFEM solution will attain the desired prescribed shape when it is subjected to service loads, and buckling is not encountered during deformation. If any of the tests fail, the IFEM output is an infeasible solution and should not be considered. Further details on these tests can be found in [13,14,33,34].

The IFEM model was implemented in the open source software GNU Octave 4.0.3 [35], built with and ad hoc configuration that includes several high performance libraries such as OpenBlas 0.2.19, Suisparse 4.5.4, ARPACK-NG 3.5.0, and LLVM-3.4 for the use of the JIT (just in time) compiler implementation for large loops.

The finite element mesh used for the IFEM analysis is depicted in Fig. 7, and it was created using the open source meshing software GMSH [36]. It is a structured quadrilateral mesh with 22000 elements, 22044 nodes, and 110220 degrees of freedom and is the best compromise between accuracy and computational cost (see [12,14]).

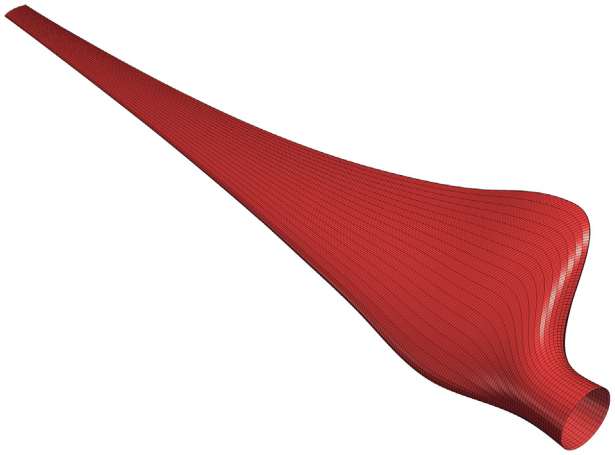

Fig. 7. Quadrilateral finite element mesh with 22000 elements, 22044 nodes, and 110220 degrees of freedom. Represents the desired shape of the blade after deformation.

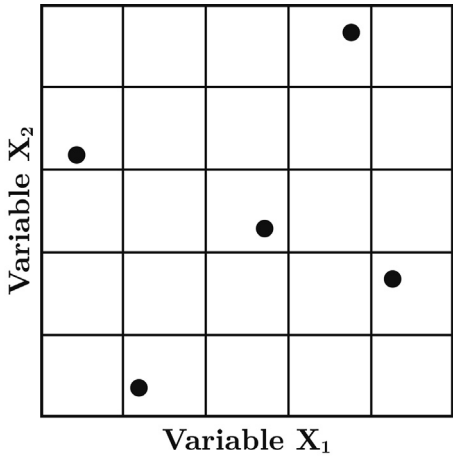

Fig. 8. Illustration of LHS for a 2-input variable problem.

3.6. Artificial neural network: training and validation

Due to the fact that multilayer feedforward networks perform a supervised learning, the data needed to train the ANN have to contain both inputs and outputs. The inputs are 19 of the 22 design variables described in Section 3.1.1 and Table 3, and were obtained through the implementation of the Latin Hypercube Sampling (LHS). The variables d_1,d_2 and d_3 were not considered because they have a fixed value of 10. The outputs are some of the design constrains explained in Section 3.1.2 related with: the maximum tip displacement defined in (4), the maximum of the stresses determined by (7)**–(12), and the frequency of the rotor described in (5) and (6). They were calculated by the IFEM simulation of the inputs.

Latin Hypercube Sampling is a technique described by McKay and Beckman [37] in which the range of each input variable is divided into N equally probable intervals, and a value from each interval is selected. Then, the selected values are matched randomly, creating a sample of size N. It is shown in Fig. 8 an example of the procedure for a sample of $N = 5$ for a 2-input variable problem. This method is widely used to construct computer design experiments because it ensures that each of the input variables has all portions of its range represented [37], no matter if the response is dominated by only a few ones [38]. Other advantages of this method are: (a) it is computationally cheap to generate; (b) it can deal with a large number of runs and input variables; (c) its sample mean has a smaller variance than the sample mean of a simple random sample.

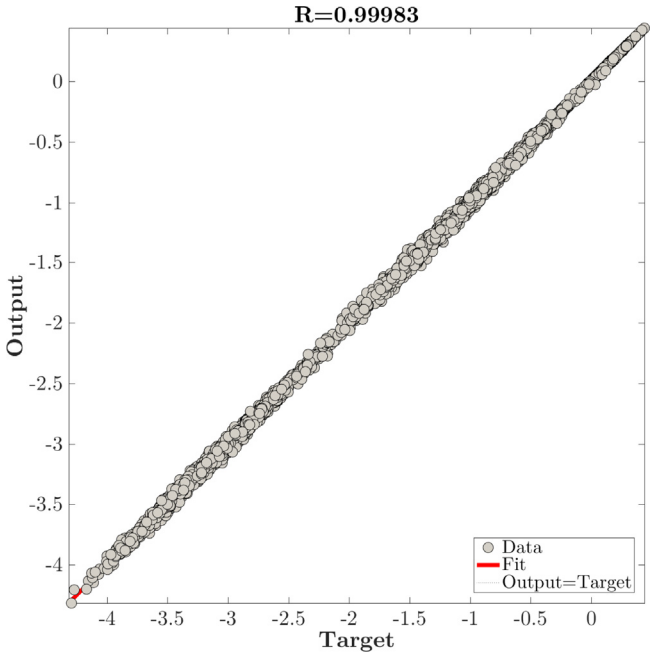

Fig. 10. Correlation coefficient for the ANN training process for all the outputs.

Three samples were created by the implementation of LHS: two for the training process of the metamodels and one for the validation of them. The size of the training samples were 2000 and 2500, and the size of the validation sample was 100. These input variables were introduced in the IFEM solver to obtain the structural response of the blades, generating the input-output samples needed to create the metamodel.

Regarding of the architecture of the metamodels, the guidelines for the development of ANN metamodels proposed by Fonseca et al. [39] were followed. Firstly, the number of hidden layers was decided by trial and error, training several architectures with the 2000 and 2500 samples. As a result, it was obtained that a two hidden layer ANN was the most appropriate configuration. Secondly, the number of neurons in each layer was calibrated by increasing it one neuron at a time. Thirdly, the ANNs that showed the best performance were chosen to validate them with the validation sample. The architecture, configuration, and parameters of the ANNs trained to replace the IFEM simulations are described in Table 4.

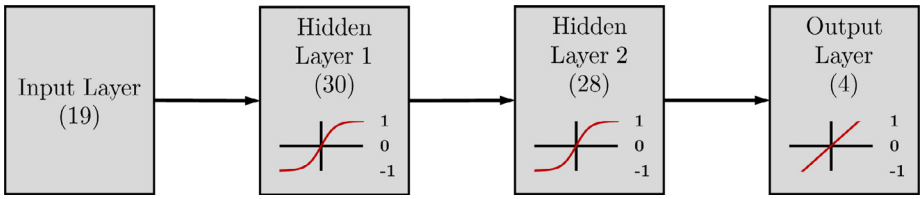

Fig. 9. Best network architecture with 30 neurons in the first hidden layer and 28 in the second one.

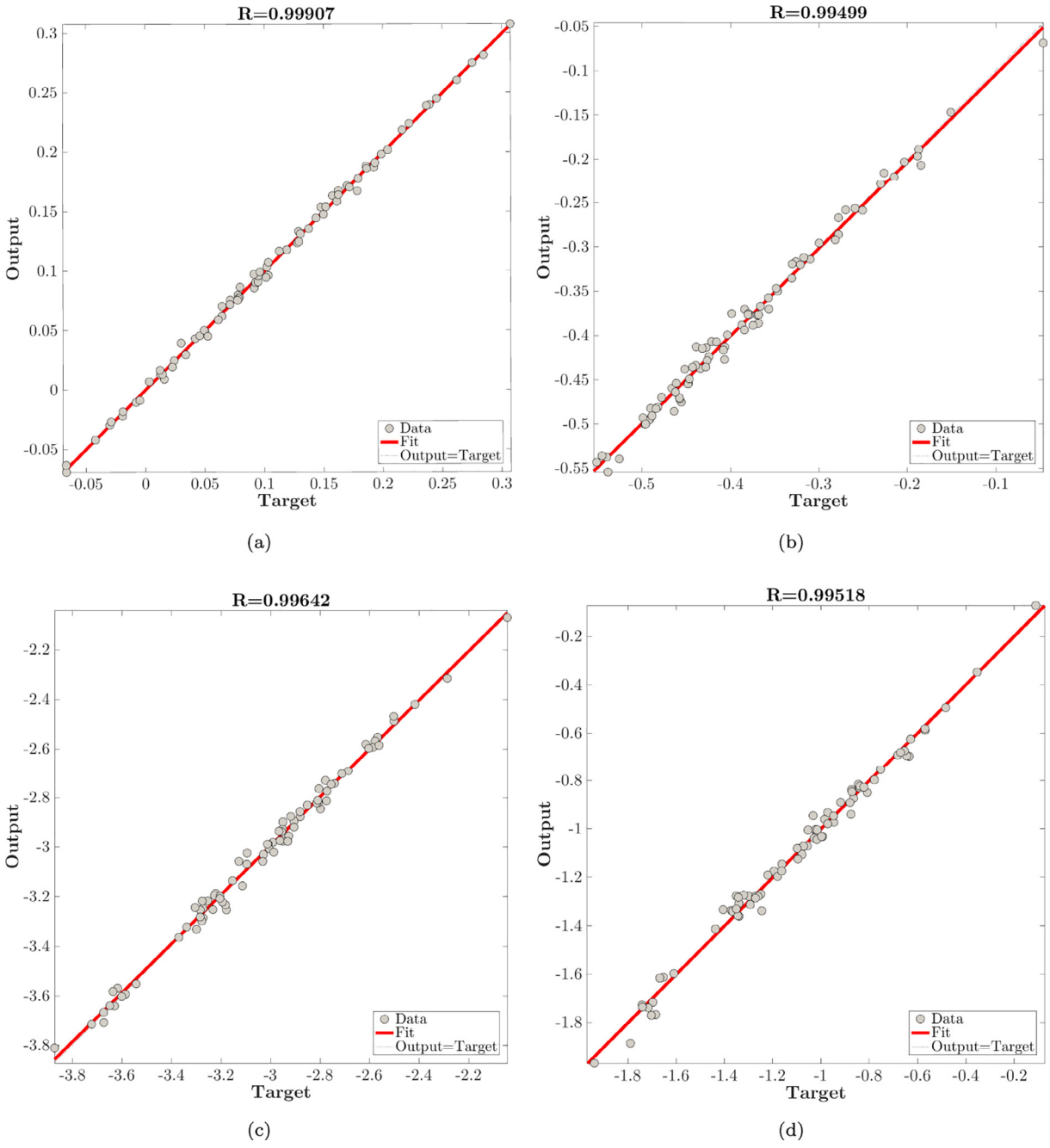

Fig. 11. Correlation coefficient for the ANN validation process. (a) Maximum tip displacement constrain; (b) Maximum stress constrain; (c) Natural frequency constrain ± 5% of f_{rot}; (d) Natural frequency constrain ± 5% of $3f_{rot}$.

Table 5
ANN metamodel approximation errors. Maximum average error (MAE), and mean square error (RMSE), of the ANN metamodel trained with 2500 sampling points.

Output	MAE	RMSE
U_{tip} [m]	0.0066734	0.008626
S_{max} [MPa]	0.28880	0.36240
$Freq_1$ [Hz]	0.34580	0.43470
$Freq_3$ [Hz]	0.35880	0.44450

Table 6
GA algorithm settings.

Parameter	Value
Number of individuals	96
Number of generations	200
Elite individuals	1
Selection	Tournament
Crossover method	Laplace
Crossover probability	100%
Mutation method	power
Mutation probability	0.5%

Table 7
Description of the optimal design variables obtained with ANN + GA. For variable m_i,$m_i = 0$ is an empty ply, $m_i = 1$ is uniaxial, $m_i = 2$ is biaxial, and $m_i = 3$ is double-bias. Variable d_i is the end region of the ply i, with $1 \leqslant d_i \leq 10$.

Description	Variable	Value
Material in layer 1	m_1	2
Material in layer 2	m_2	2
Material in layer 3	m_3	2
Material in layer 4	m_4	1
Material in layer 5	m_5	2
Material in layer 6	m_6	2
Material in layer 7	m_7	3
Extension of layer 1	d_1	10
Extension of layer 2	d_2	10
Extension of layer 3	d_3	10
Extension of layer 4	d_4	7
Extension of layer 5	d_5	8
Extension of layer 6	d_6	9
Extension of layer 7	d_7	9

4. Results and discussion

4.1. ANN results

The best network architecture had 30 neurons in the first hidden layer and 28 in the second one, as illustrated in Fig. 9. It was trained with 2500 IFEM sampling points and validated with 100 sampling points. The training correlation factor for all the outputs is R = 0.99983, and the validation correlation factors of each output are between 0.99499 and 0.99907 which give an excellent agreement as it is shown in Figs. 10 and 11. Table 5 presents the maximum average error (MAE), and mean square error (RMSE) of this ANN for all outputs.

4.2. Optimization results

The best-trained and validated ANN model is used as the objective function in the optimization task, coupling this ANN model with the GA presented before. GA settings (population size, selection, crossover and mutation methods, the probability of mutation and crossover, etc.) depend on the characteristics of the optimization problem [40]. In this case, the results were obtained for the GA configuration shown in Table 6. Note that because the low time of ANN evaluation, was possible to make an exhaustive optimization analysis (with a bigger size of the population and more generations than the direct coupling GA + IFEM) in order to find the global minimum or one nearly to it.

4.2.1. Optimal design

Using the combination of ANN + GA, the optimal blade weighs 22.85 kg, being 20% lighter than the reference blade (28.82 kg) and 6% lighter that the former design with IFEM + GA (24.48 kg). The resulting material layout in the shell skin of the blade consists in a total of 6 layers (besides the outer gelcoat ply) having the stacking sequence (from the core): biaxial/biaxial/biaxial/uniaxial/biaxial/biaxial/double-bias. The optimal design variables are listed in Table 7.

Fig. 12 shows the laminated of the optimal design found and the comparison with others results obtained in previous works. The current laminate (Fig. 12a) represents a reduction of 5 layers compared to the

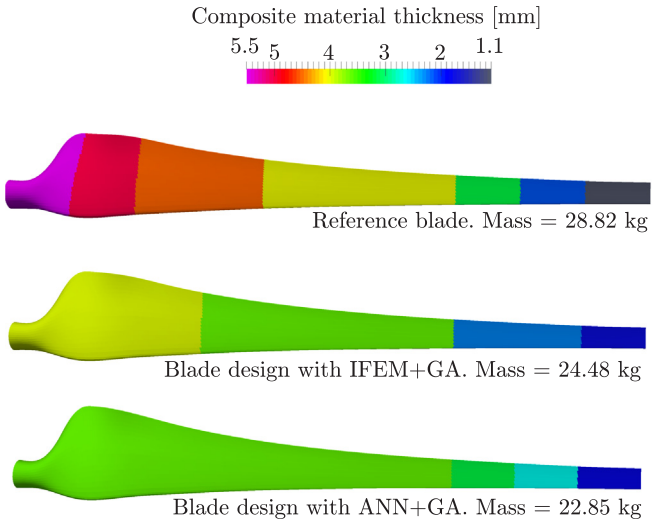

Fig. 13. Thickness of the laminated composite material in the shell skin of the optimal design.

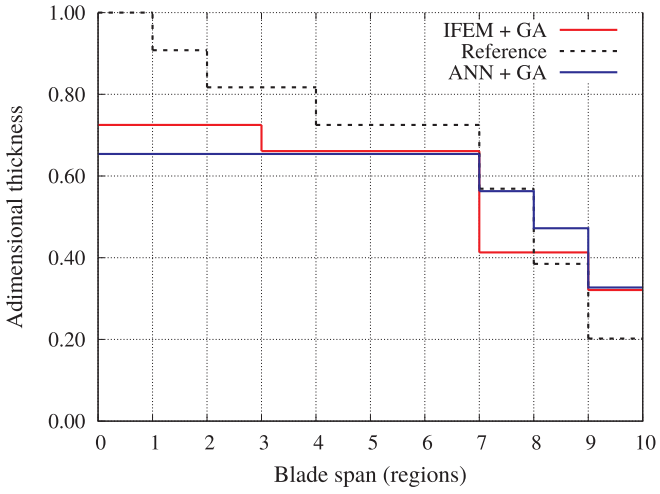

Fig. 14. Adimensional thickness of the shell skin for the reference and optimal designs.

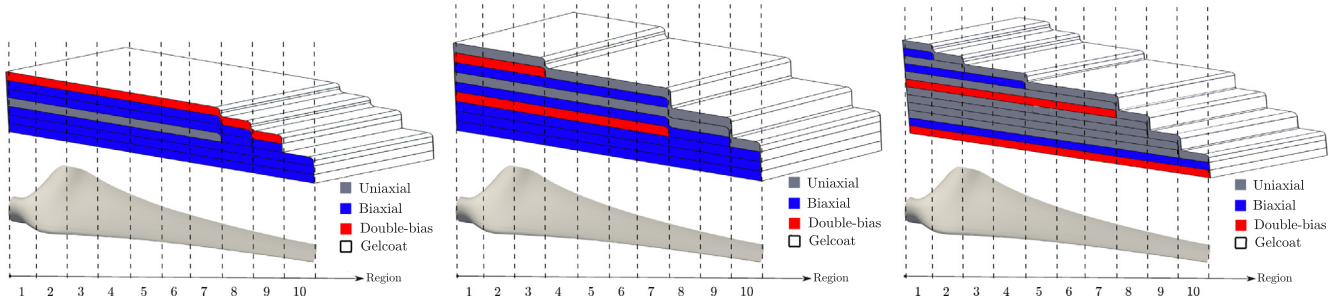

Fig. 12. (a) Resulting material layout in the shell skin of the blade obtained with ANN + GA method; (b) Design obtained with IFEM + GA; (c) Design obtained with IFEM and user's calibration.

Table 8
Maximum and minimum principal stresses (σ_1 and σ_2) and shear stress τ_{12}, measured in [MPa]. All values are below 100 [MPa], ensuring that stresses remain in the linear elastic regime.

Ply	Material	maxσ_1	minσ_1	maxσ_2	minσ_2	maxτ_{12}	minτ_{12}
1	Biaxial	89.54	−20.98	43.22	−44.67	27.01	−27.01
2	Biaxial	71.38	−15.12	36.22	−39.77	22.07	−22.07
3	Biaxial	69.21	−18.88	32.37	−39.91	25.08	−25.08
4	Uniaxial	49.07	−6.62	8.92	−39.73	22.31	−22.31
5	Biaxial	55.84	−17.13	14.76	−34.28	26.22	−26.22
6	Biaxial	51.65	−17.87	22.26	−59.38	44.32	−44.32
7	Double-bias	43.37	−21.78	27.34	−67.59	37.30	−37.30

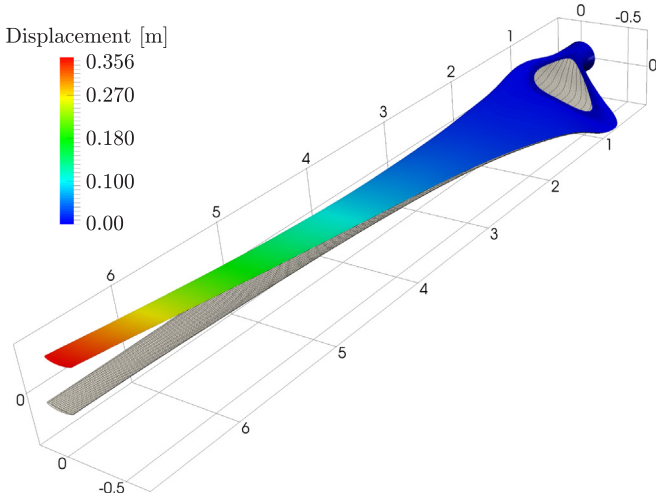

Fig. 15. Displacement modulus in the optimized blade. The prescribed aerodynamic geometry is plotted in wireframe. The tip displacement in the optimized blade is only 0.006 m larger than the admissible tip displacement $u_{max} = 0.350$ m.

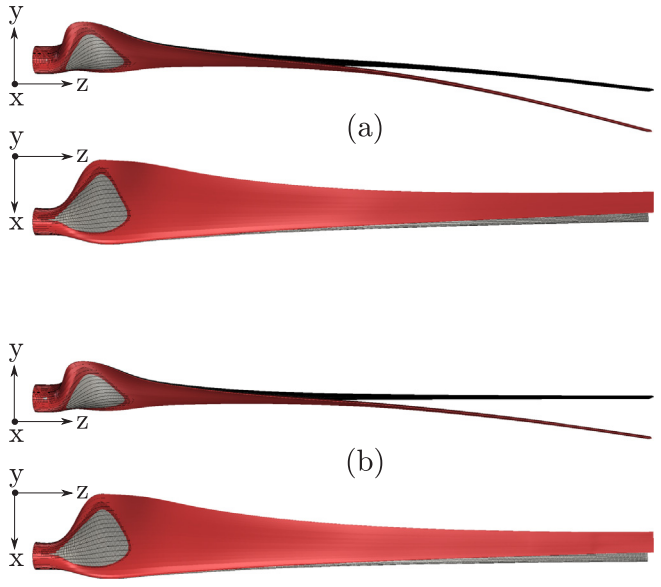

Fig. 16. First natural mode of vibration (4.3932 Hz), flapwise predominant. (a) depicted for the manufacturing shape of the blade; (b) depicted for the loaded shape of the blade. Represented by the color surface and amplified by a factor of 30.

reference design (Fig. 12c) [14], and of 2 layers compared to the design obtained using IFEM + GA (Fig. 12b) [12]. It also has a lower number of ply drops compared to the previous designs and has less variation of

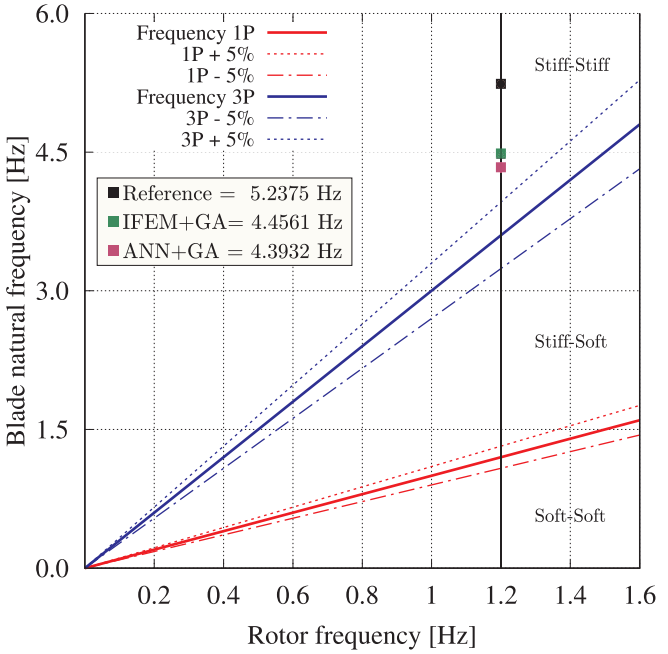

Fig. 17. Campbell diagram regarding blade vibrations.

Table 9
Comparison between the reference, former IFEM + GA design, and current ANN + GA optimal designs.

Characteristic	Reference	IFEM + GA	ANN + GA
Number of plies	11	9	7
Blade weight	28.82 kg	24.28 kg	22.85 kg
Tip deflection	0.3500 m	0.3425 m	0.3560 m
1st eigenvalue	5.8575 Hz	4.4561 Hz	4.3932 Hz

material in the laminate thickness. In addition to the weight reduction, this fact also implies that the laminate would be easier and cheaper to manufacture. We note that some regions may be longer than the inner layers without losing continuity, see reference [23].

Fig. 13 compares the thickness of the laminated composite material in the shell skin of the designs, i.e., the reference, the former optimized design obtained with IFEM + GA, and the current optimal design obtained with ANN + GA. Fig. 14 shows the comparison between the adimensional thickness of the shell skin for the reference and optimal wind turbine blade designs.

4.2.2. Design constraints

Besides satisfying all the manufacturing constraints, $\boldsymbol{x}_{opt}$ also must satisfy all the mechanical constraints. To validate this latter, the optimal design found ($\boldsymbol{x}_{opt}$) is evaluated using the accurate IFEM simulation.

4.2.2.1. Maximum stress failure criterion. Regarding the maximum stresses, this can be assessed by comparing those listed in Table 8 with their thresholds (dependent on the material of the ply) given in Table 2. Since the values of Table 8 are below 100 [MPa], all stresses remain in the linear elastic regime for a composite made of E-type glass fiber and epoxy resin [41,42].

4.2.2.2. Maximum deflection of the blade. Fig. 15 depicts the computed manufacturing shape of the blade with the new laminate using IFEM. As it can be observed, the tip displacement in the optimized blade is $u_{tip} = 0.356$ m, only 0.006 m larger than the admissible tip displacement $u_{max} = 0.350$ m of the inequality constraint (4). Hence, the error in

displacement is only 1.71%, which we consider a negligible value compared to the mass reduction of 20% achieved with the current procedure.

4.2.2.3. Vibration of the blades. The first natural frequency constraint of the optimal design is 4.3932 Hz, quite far from the frequency of the rotor $f_{rot} = 1.2$ Hz and $3f_{rot} = 3.6$ Hz, in which case resonance is avoided. The first natural vibration mode for the optimal blade is illustrated in Fig. 16 for both the unloaded (manufacturing) and loaded shapes (service shape).

In Fig. 17 the Campbell diagram for all of the blades considered in this work is represented. The vertical axis corresponds to the natural frequency of the blades, and the horizontal axis is the operation range of the turbine (rotation frequency of the rotor) [43]. The main regions of this plot are the exclusion windows representing the rotation constraint $f_{rot} \pm 5\%$ and bladepassing constraint $3f_{rot} \pm 5\%$ along the operating range of the rotor. It can be seen that resonance is avoided since the vertical line representing the rotation frequency of the rotor ($f_{rot} = 1.2$) does not cross any of the exclusion windows. Also, all blades lie in the stiff-stiff region of the diagram, in which case a very stiff foundation is required [44]. This is because the stiffening effect due to the rotation is very important small and medium-sized wind turbines [45,46].

4.2.2.4. Computational cost. In order to compare the computational cost between ANN + GA and IFEM + GA, the total IFEM simulations used in each method is considered. Although two different sample sizes (2000 and 2500, which gives a total of 4500 IFEM simulations) were tested to get an accurate ANN model, it was demonstrated that with the correct size sample (2500) it is possible to get accurate optimization results. On the other hand, the short computational time of the ANN evaluation used by ANN + GA method allowed to run an exhaustive optimization and to find a better optimal design than the IFEM + GA approach.

4.2.2.5. Summary results. Finally, Table 9 compares the main characteristics of the optimal and the reference blades.

5. Conclusion

In this work, a new metamodel-based optimization approach to redesign the composite laminate of wind turbine blades was presented. The method combines a genetic algorithm (GA) with an artificial neural network (ANN) model to achieve the simultaneous optimal ply-order, ply-number, and ply-drop of the composite materials. Finally, the method was applied to the redesign of a medium-power 40-kW wind turbine blade to minimize its mass while structural and manufacturing constraints are fulfilled.

The Latin Hypercube Sampling technique proved to be an adequate method to obtain a representative sample of 2500 designs, out of a total 1.8×10^{14} possible laminate configurations. The ANN model trained with this sample showed an excellent agreement between the inverse finite element method (IFEM) structural solver and the metamodel prediction, attaining correlation coefficients above 0.99 for each constraint.

The use of the ANN model in the current optimization task allowed a 40% reduction of the computational cost in contrast with the typical simulation-based optimization approach if the correct sample size is chosen. Further, because of the short computational time consumed by the ANN evaluation in this ANN + GA procedure, a more exhaustive optimization was possible, and savings of up to 20% (5% better than IFEM + GA) of laminated mass was achieved compared to a reference design.

Future work will be focused on extending the proposed method to bigger wind turbine blades with more complex laminate configurations (for instance different fiber orientations), more detail in the manufacturing technology (including for example shear webs and spar caps), and manufacturing costs. Moreover, multi-objective optimization will be considered to take into account naturally contradictory objectives, like the weight and stiffness of the laminated blade.

Acknowledgments

The authors gratefully acknowledge the financial support from CONICET (Argentine Council for Scientific and Technical Research). A. E. Albanesi also acknowledges the National Technological University of Argentina (UTN) for Grants PID 4405 and PID 2425, and the National Agency of Scientific and Technological Promotion of Argentina (ANPCYT) for the Grant PICT 3396.

References

[1] Burton T, Jenkins N, Sharpe D, Bossanyi E. Wind Energy Handbook. 2nd ed. John Wiley and Sons; 2011.
[2] Ghiasi H, Pasini D, Lessard L. Optimum stacking sequence design of composite materials Part I: Constant stiffness design. Compos Struct 2009;90:1–11.
[3] Ghiasi H, Fayazbakhsh K, Pasini D, Lessard L. Optimum stacking sequence design of composite materials Part II: Variable stiffness design. Compos Struct 2010;93:1–13.
[4] Dey S, Mukhopadhyay T, Adhikari S. Metamodel based high-fidelity stochastic analysis of composite laminates: A concise review with critical comparative assessment. Compos Struct 2017;171(Supplement C):227–50.
[5] Yan F, Lin Z, Wang X, Azarmi F, Sobolev K. Evaluation and prediction of bond strength of GFRP-bar reinforced concrete using artificial neural network optimized with genetic algorithm. Compos Struct 2017;161(0):441–52.
[6] Artero-Guerrero JA, Pernas-Sánchez J, Martín-Montal J, Varas D, López-Puente J. The influence of laminate stacking sequence on ballistic limit using a combined Experimental/FEM/Artificial Neural Networks (ANN) methodology. Compos Struct 2018;183(Supplement C):299–308. In honor of Prof. Y. Narita.
[7] Balokas Georgios, Czichon Steffen, Rolfes Raimund. Neural network assisted multiscale analysis for the elastic properties prediction of 3d braided composites under uncertainty. Compos Struct 2018;183(Supplement C):550–62. In honor of Prof. Y. Narita.
[8] Bisagni C, Lanzi L. Post-buckling optimisation of composite stiffened panels using neural networks. Compos Struct 2002;58(2):237–47.
[9] Fu X, Ricci S, Bisagni C. Minimum-weight design for three dimensional woven composite stiffened panels using neural networks and genetic algorithms. Compos. Struct. 2015;134(Supplement C):708–15. ISSN 0263-8223.
[10] Abouhamze M, Shakeri M. Multi-objective stacking sequence optimization of laminated cylindrical panels using a genetic algorithm and neural networks. Compos Struct 2007;81(2):253–63.
[11] Marín L, Trias D, Badall P, Rus G, Mayugo JA. Optimization of composite stiffened panels under mechanical and hygrothermal loads using neural networks and genetic algorithms. Compos Struct 2012;94(11):3321–6.
[12] Albanesi A, Bre F, Fachinotti V, Gebhardt C. Simultaneous ply-order, ply-number and ply-drop optimization of laminate wind turbine blades using the inverse finite element method. Compos Struct 2017;184:894–903.
[13] Fachinotti VD, Albanesi AE, Martínez Valle JM. Inverse finite element modeling of shells using the degenerate solid approach. Comput Struct 2015;157:89–98.
[14] Albanesi A, Fachinotti V, Peralta I, Storti B, Gebhardt C. Application of the inverse finite element method to design wind turbine blades. Compos Struct 2016;161:160–72.
[15] Giguere PP, Selig MS. New airfoils for small horizontal axis wind turbines. ASME J Sol Energy Eng 1998;120(2):108–14.
[16] Zein S, Madhavan V, Dumas D, Ravier L, Yague I. From stacking sequences to ply layouts: an algorithm to design manufacturable composite structures. Compos Struct 2016;141:32–8.
[17] Liu D, Toropov VV, Zhou M, Barton D, Querin O. Optimization of Blended Composite Wing Panels Using Smeared Stiffness Technique and Lamination Parameters. In: 51st AIAA/ASME/ASCE/AHS/ASC Structures, Structural Dynamics, and Materials Conference; 2010.
[18] Niu MCY. Airframe structural design. 2nd ed. Conmilit Press Ltd; 1999.
[19] Barbero EJ. Introduction to composite materials design. 2nd ed. CRC Press; 2011.
[20] Kaw AK. Mechanics of composite materials. 2nd ed. CRC Press; 2006.
[21] Jones R. Mechanics of composite materials. 2nd ed. Taylor and Francis; 1999.
[22] Irisarri F-X, Lasseigne A, Leroy F-H, Le Riche R. Optimal design of laminated composite structures with ply drops using stacking sequence tables. Compos Struct 2014;107:559–69.
[23] Fan H-T, Wang H, Chen X-H. An optimization method for composite structures with ply-drops. Compos Struct 2016;136:650–61.
[24] Wang L, Kolios A, Nishino T, Delafin P-L, Bird T. Structural optimisation of vertical-axis wind turbine composite blades based on finite element analysis and genetic algorithm. Compos Struct 2016;153:123–38.
[25] Dal Monte A, Castelli MR, Benini E. Multi-objective structural optimization of a HAWT composite blade. Compos Struct 2013;106:362–73.
[26] Fagan EM, Flanagan M, Leen SB, Flanagan T, Doyle A, Goggins J. Physical experimental static testing and structural design optimisation for a composite wind turbine blade. Compos Struct 2017;164:90–103.

[27] Deep K, Singh KP, Kansal ML, Mohan C. A real coded genetic algorithm for solving integer and mixed integer optimization problems. Appl Math Comput 2009;212(2):505–18.
[28] Bre F, Fachinotti VD. A computational multi-objective optimization method to improve energy efficiency and thermal comfort in dwellings. Energy Build 2017;154(Supplement C):283–94. ISSN 0378-7788.
[29] Simpson TW, Peplinski J, Koch PN, Allen JK. Metamodels for computer-based engineering design: survey and recommendations. National Aeronautics and Space Administration; 1997. Technical report.
[30] Haykin Simon. Neural networks: a comprehensive foundation. 2nd ed. Pearson Education; 1999.
[31] Fausett Laurene V. Fundamentals of neural networks. us ed edition Prentice Hall; 1993. ISBN 9780133341867,0133341860.
[32] Dvorkin EN, Bathe K-J. A continuum mechanics based four-node shell element for general nonlinear analysis. Eng Comput 1984;1:77–88.
[33] Albanesi AE, Pucheta MA, Fachinotti VD. A new method to design compliant mechanisms based on the inverse beam finite element model. Mech Mach Theory 2013;65:14–28.
[34] Albanesi AE. Inverse design methods for compliant mechanisms. Santa Fe, Argentina: Faculty of Engineering and Water Sciences, National Littoral University; 2011. (Ph.D. thesis).
[35] Eaton JW, Bateman D, Hauberg S, Wehbring R. GNU Octave version 4.0.3 manual: a high-level interactive language for numerical computations; 2016. URLhttp://www.gnu.org/software/octave/doc/interpreter.
[36] Geuzaine C, Remacle J-F. Gmsh: a three-dimensional finite element mesh generator with built-in pre-and post-processing facilities. Int J Numer Meth Eng 2009;79(11):1309–31.
[37] McKay MD, Beckman RJ. A comparison of three methods for selecting values of input variables in the analysis of output from a computer code. Technometrics 1979;21(2):239–45.
[38] Fang K-T, Li R, Sudjianto A. Design and modeling for computer experiments. CRC Press; 2005.
[39] Fonseca DJ, Navaresse DO, Moynihan GP. Simulation metamodeling through artificial neural networks. Eng Appl Artif Intell 2003;16(3):177–83.
[40] Deb K. An efficient constraint handling method for genetic algorithms. Comput Methods Appl Mech Eng 2000;18:311–38.
[41] Belingardi G, Paolino DS, Koricho EG. Investigation of influence of tab types on tensile strength of E-glass/epoxy fiber reinforced composite materials. Procedia Eng 2011;10:3279–84.
[42] Elanchezhian C, Vijaya Ramnath B, Hemalatha J. Mechanical behaviour of glass and carbon fibre reinforced composites at varying strain rates and temperatures. Procedia Mater Sci 2014;6:1405–18.
[43] Petersen B, Pollack M, Connell B, Greeley D, Daivis D, Slavik C. Evaluate the effect of turbine period of vibration requirements on structural design parameters. Appl Phys Sci 2010. Technical report.
[44] Andersen LV, Vahdatirad MJ, Sichani MT, Srensen JD. Natural frequencies of wind turbines on monopile foundations in clayey soils A probabilistic approach. Comput. Geotech. 2012;43(Supplement C):1–11.
[45] Gebhardt CG, Roccia BA. Non-linear aeroelasticity: an approach to compute the response of three-blade large-scale horizontal-axis wind turbines. Renewable Energy 2014;66:495–514.
[46] Holm-Jrgensen K, Nielsen SRK. A component mode synthesis algorithm for multibody dynamics of wind turbines. J Sound Vibr 2009;326:753–67.